ChemPubSoc Europe

DOI: 10.1002/cphc.201700583

CHEMPHYSCHEM Communications

VIP *Very Important Paper*

Special Issue

Diagnosing the Internal Architecture of Zeolite Ferrierite

Joel E. Schmidt,[a] Frank C. Hendriks,[a] Martin Lutz,[b] L. Christiaan Post,[c] Donglong Fu,[a] and Bert M. Weckhuysen*[a]

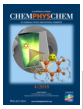

Large crystals of zeolite ferrierite (FER) are important model systems for spatially resolved catalysis and diffusion studies, though there is considerable variation in crystal habit depending on the chemical composition and employed synthesis conditions. A synergistic combination of techniques has been applied, including single crystal X-ray diffraction, high-temperature in situ confocal fluorescence microscopy, fluorescent probe molecules, wide-field microscopy and atomic force microscopy to unravel the internal architecture of three distinct FER zeolites. Pyrolyzed template species can be used as markers for the 8-membered ring direction as they are trapped in the terraced roof of the FER crystals. This happens as the materials grow in a layer-by-layer, defect-free manner normal to the large crystal surface, and leads to a facile method to diagnose the pore system orientation, which avoids tedious single crystal X-ray diffraction experiments.

Microporous materials form a critical pillar of the world's current manufacturing and production industries as they are used in diverse applications including oil refining, separations, water treatment, emissions reduction and nuclear waste remediation.[1–7] Decades of industrial utilization have ensured that interest in these materials remains from both academic and application-driven perspectives. Fundamental insight into these materials is complicated by their small size (crystals are commonly less than one micron), the tendency for materials to crystalize as complex intergrowths and their susceptibility to electron beam damage.[8] Most studies are therefore conducted on bulk materials, where the insights gained reflect only macroscopic properties.[9] One method to overcome this barrier has been the use of large zeolite crystals, which enable spatially resolved studies that give structure-property relationships. Perhaps the most investigated system is that of large zeolite ZSM-5 crystals, which have given numerous insights into structural and compositional inhomogeneities that exist within single zeolite crystals.[10–15]

Zeolite ferrierite (FER) can be synthesized as large, defect-free single crystals. Its structure contains a 2D system of intersecting pores limited by 8- and 10-membered rings (MRs), and is nonporous in the third direction. FER is used industrially, with olefin oligomerization as the largest reported catalytic application.[7] The synthesis of very large (>100 μm) single crystals of FER was first reported in the pioneering work of Kuperman et al.[16] Large FER crystals have a plate-like morphology and can be prepared as defect-free, purely siliceous materials, as well as catalytically active aluminosilicates and borosilicates. This has led to notable studies including diffusion through a single pore orientation,[17] spatiotemporal diffusion measurements[18–22] and pore-mouth catalysis.[23] The range of crystal habits and aspect ratios are dependent on the specific synthesis conditions and compositions, and the crystals also have a domed roof with a flat pyramidal morphology as shown in Figure 1c.[16,24–26] A key feature of these materials that has enabled many of the aforementioned investigations is that the 8- and 10-MRs run along the long dimensions of the crystal, and the top and bottom crystal faces are impermeable. However, the orientation of the 8- and 10-MRs with respect to the length and width of the crystal is dependent on the exact synthesis composition and batch, as is illustrated in Figure 1.[24,25,27,28] As important conclusions are routinely drawn based on the size discrimination of 8- versus 10-MRs, it is important that their orientation with respect to crystal habit can be readily established without the need for demanding single crystal X-ray studies.

Herein, we report on investigations of a set of large FER crystals using a variety of techniques to achieve a global view of these materials, including their pore orientation, growth mechanism, and presence of crystalline defects. The pyrolyzed template molecules, unable to escape through 8-MRs in the roof section of the crystals, are leveraged as markers of pore orientation using confocal fluorescence microscopy (CFM). Complementary information can be obtained on calcined materials using fluorescent probe molecules, with the added benefit that they are an effective method of quickly screening for crystalline defects. Using atomic force microscopy (AFM), it was found that the large crystals contain terraces with a half unit cell step, containing a single exposed layer of 8- and 10-

[a] Dr. J. E. Schmidt, F. C. Hendriks, D. Fu, Prof. Dr. B. M. Weckhuysen
Inorganic Chemistry and Catalysis Group
Debye Institute for Nanomaterials Science, Utrecht University
Universiteitsweg 99, 3584 CG Utrecht (The Netherlands)
E-mail: b.m.weckhuysen@uu.nl

[b] Dr. M. Lutz
Crystal and Structural Chemistry
Bijvoet Center for Biomolecular Research, Utrecht University
Padualaan 8, 3584 CH Utrecht (The Netherlands)

[c] L. C. Post
Condensed Matter and Interfaces
Debye Institute for Nanomaterials Science, Utrecht University
Princetonplein 1, 3584 CC Utrecht (The Netherlands)

Supporting Information and the ORCID identification number(s) for the author(s) of this article can be found under: https://doi.org/10.1002/cphc.201700583.

An invited contribution to a Special Issue on Reactions in Confined Spaces

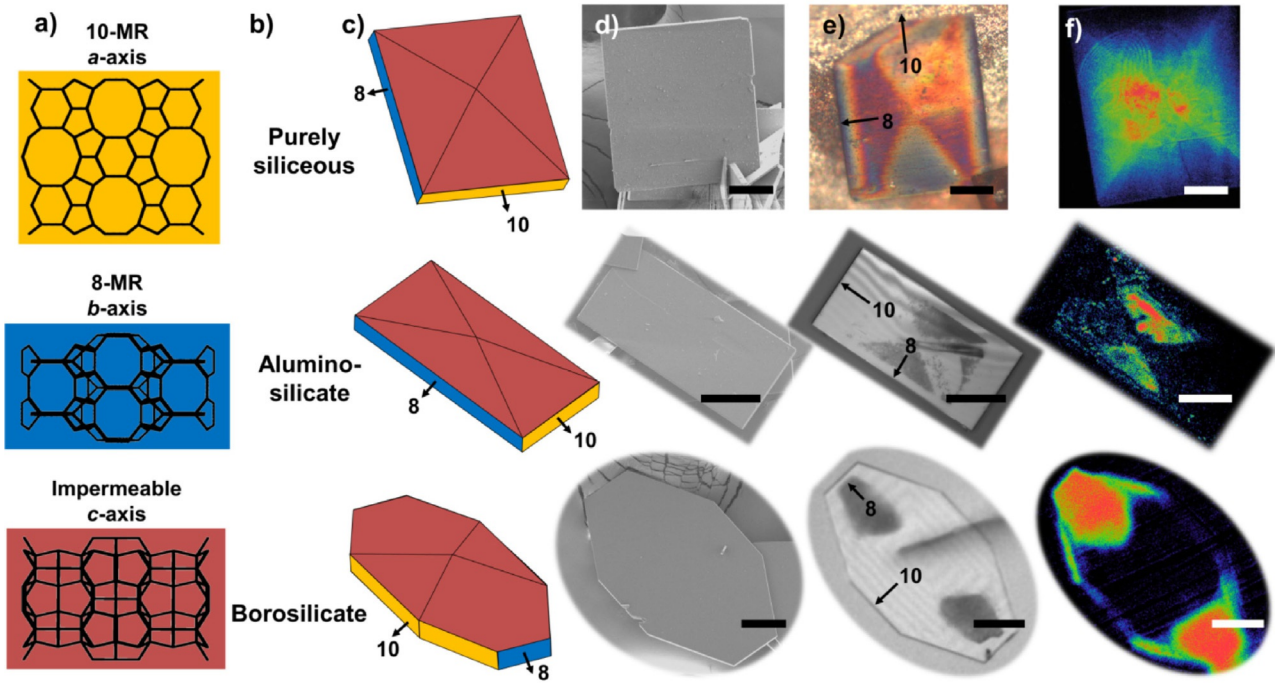

Figure 1. Overview of the different crystal morphologies as well as characterization techniques used in this study for the three different compositions of zeolite ferrierite (FER), shown across each row. a) Pore system down each of the three crystallographic directions. b) Composition of the crystal in each row for the three samples studied, as detailed in Table 1. c) Schematic representations of the morphologies of the three different samples used in this study, colors correspond to the different crystallographic directions in a, and the pore directions are also indicated. The crystal thickness has been exaggerated for clarity. d) Scanning electron microscopy (SEM) images of the three different samples. e) Optical microscopy images of the three different samples showing triangular regions in each crystal containing pyrolyzed organic template, directions of the 8- and 10-membered rings are indicated. f) Confocal fluorescence microscopy (CFM) images of (top) template containing large purely siliceous FER crystals recorded at 600 °C in an in situ cell, with birefringence visible (concentric circles) caused by internal pressure due to occluded organic species that are unable to escape. (middle) Aluminosilicate FER that contains residual pyrolyzed organic template species after calcination, recorded at 500 °C in an in situ cell in a N_2 atmosphere. (bottom) Borosilicate FER that contained residual pyrolyzed organic template species after calcination, the image was recorded at room temperature. All scale bars represent 50 μm.

MRs per terrace. This terracing is consistent with a layer-by-layer growth mechanism that leads to trapped template molecules, and explains the correlation between trapped species and pore orientation used in this paper to easily diagnose the pore orientation of FER crystals.

Upon examination of calcined, large crystals of aluminosilicate and borosilicate FER, it was observed that some crystals contained regular dark patches, with representative images in Figure 1e. In the aluminosilicate material, with a rectangular morphology, the long edge of these dark triangular regions coincides with the longest crystal edge, which contains the opening of the 8-MRs as depicted in Figure 1c and was recently reported on by Wiedemann et al.[23] To the best of our knowledge, there are no reports specifically studying the pore orientation with respect to crystal habit in a borosilicate FER material, so it was not possible to make a correlation of the dark region with a certain pore direction. The opening of the 10-MRs in the purely siliceous material is reported to be at either the longest edge[27] (length) or second longest edge[24] (width) in two separate single crystal studies on different samples of purely siliceous FER. These conflicting observations motivated us to explore the pore orientation with respect to crystal habit in detail and to understand the origin of the dark patches in the crystals, which were presumably from pyrolyzed organic template molecules that remained occluded due to incomplete calcination of zeolite FER crystals.

Three distinct ferrierite samples were considered, encompassing purely siliceous, aluminosilicate and borosilicate materials, with sample details given in Table 1. These crystals exhibited different morphologies and were prepared using different synthetic protocols in two separate laboratories, allowing us to examine a diverse range of materials. Representative images of each sample from both SEM and light microscopy are included in Figure 1. The purely siliceous and aluminosilicate materials have a rectangular morphology, though with different aspect ratios, while the borosilicate material has an octagonal morphology.

The orientation of the pores with respect to crystal habit was unambiguously determined in each sample by single crystal X-ray structure analysis, and the experimental method and full results are given in the Supporting Information, Section S1,

Table 1. Description of FER samples under investigation.

Sample number	Description	Composition	Synthesis method	Sample source
1	with template	purely siliceous	Ref. [16]	Pasadena
2	without template	Si/Al = 23	Ref. [24]	Stuttgart
3	without template	Si/B = 108	Ref. [24]	Stuttgart

and the results are shown in Figure 1. The unit cell sizes are given in Table S1, and the analysis is in good agreement with previous reports, with small changes in the unit cell size depending on the composition.[27,29–34] Herein, we are using the standard space group setting of $a < b < c$, and in this description the *a*-axis is the direction of the 10-MRs, the *b*-axis is the direction of the 8-MRs and the *c*-axis is impermeable.[27] In the purely siliceous and aluminosilicate materials, with a rectangular morphology, the 10-MRs open at the short edge of the crystals, while the 8-MRs open at the long edge of the crystals. In octagonal, borosilicate crystals, the orientation is reversed, with the 10-MRs opening at the long edge of the crystals and the 8-MRs at the short edge. These results show that crystal morphology alone is not a good indicator of pore orientation, as the locations of the 8- and 10-MRs with respect to the length and width can indeed vary substantially. Therefore, a simple method to determine internal pore orientation would be beneficial and has been developed in this work.

Our group has been developing CFM under in situ conditions to elucidate the internal crystallographic intergrowth structure by monitoring fluorescent species during the template removal process at high temperature for AFI, CHA, and MFI frameworks.[10,35–37] In the present work we applied this same method to template-containing crystals of purely siliceous FER (**1**), by heating them under a N_2 atmosphere to 600 °C. A CFM image recorded at 500 °C is shown in Figure 1 f, and distinct fluorescent regions with a triangular shape are visible. These triangular regions have their long edge parallel to the side of the crystals at which the 8-MRs are open. A previous thermogravimetric analysis (TGA) study showed that the pyridine template could be easily removed from the 10-MR channel below 417 °C, but that fully removing pyridine from the 8-MR side-pockets required calcination in dry oxygen at 800 °C for 48 h.[31] It is therefore likely the fluorescence is caused by trapped light-absorbing organic molecules that cannot be easily removed through the 8-MRs, and their presence is evident in the crystals at high temperature as they cause the birefringence in Figure 1 f.[28] Samples of the aluminosilicate (**2**) and borosilicate FER (**3**) containing dark patches were then studied in a similar manner with CFM, with the 2D CFM maps shown in Figure 1 f. Similar fluorescent behavior was observed in both of these samples, confirming that the dark patches are indeed pyrolyzed template molecules and that this fluorescence is a general attribute of these large zeolite FER crystals due to pyrolyzed template molecules.

After heating to 600 °C in a N_2 atmosphere, the crystals of template containing purely siliceous FER (**1**), were cooled to room temperature. In some of the zeolite crystals, a distinct coloration pattern was observed (Figure 1 e). Dark triangular regions were found in the same location as the fluorescence, meaning that pyrolysis leaves dark carbonaceous species that can serve as a marker for the pore direction, similar to the triangular regions of pyrolyzed template species that resulted from incomplete calcination that were found in samples **2** and **3**. The dark patches identified in these crystals are consistent with the roof sections containing the 8-MRs as determined using single crystal X-ray diffraction. Therefore, incomplete calcination or pyrolysis results in occluded, pyrolyzed carbon deposits that can be used as a marker for 8-MRs in large FER crystals without having to resort to single crystal diffraction studies.

In a next step of our study, we have applied the fluorescent probe molecule DAMPI, shown in Figure S4, as it is known to fit into 10-, but not 8-MRs.[38,39] Calcined crystals of all three zeolite FER samples were treated with ethanolic solutions of DAMPI, and then studied using CFM, as detailed in the Supporting Information Sections S2 and S3. The results of the CFM study using DAMPI are shown in Figure 2. In all three samples an accumulation of DAMPI molecules is found at the opening of the 10-MRs, simultaneously demonstrating i) additional confirmation of the pore orientation and ii) that the 10-MRs are accessible and not blocked. Another benefit of studying the crystals using probe molecules is that these are highly sensitive to any material defects arising from mechanical damage or crystalline intergrowths.[39] Further examination of Figure 2 a shows significant fluorescence in distinct regions of the crystal, which coincide with the mechanical damage to the crystal. A damaged crystal was chosen to demonstrate that DAMPI molecules would accumulate in defects, even in a neutral framework, as is the case with purely siliceous FER crystals. The other two zeolite materials did not show any significant internal fluorescence, leading to the conclusion that there are no accessible defects. While this may seem obvious due to the regular nature of these crystals, our recent study of large MFI crystals showed that DAMPI can highlight internal intergrowth structures, demonstrating that large FER crystals do not contain these features.[39] Thus, the fluorescent probe molecule is able to highlight the location of the 10-MRs, as well as reveal physical damage to the zeolite crystals. The results show the susceptibility of these large crystals to physical damage, and the importance of carefully treating them (e.g. during calcination and manual manipulation).

The CFM results of purely siliceous FER (**1**) were revisited and examined in 3D, as shown in Figure 3 a, and it was found that the fluorescent regions were only present in the roof of the crystal (Figure 3 a). The existence of this roof region has been previously reported, and led to interesting results when studying methanol diffusion with interference microscopy. Fast diffusion was observed in the roof as compared to the main body of the crystal, due to open 8- or 10-MRs along the pitch of the roof as methanol can readily escape through both.[19,27,28] When the results of the 3D CFM study are combined with this view of the crystal roof, a deeper understanding of the interconnectivity of the internal pore system emerges, with distinct regions in the crystal: i) In the main body of the crystal the 8- and 10-MRs are fully interconnected with no faults to block the pores, which is why only minimal fluorescence was observed in the center of the crystal as the template molecules were able to diffuse out. ii) In the fluorescent roof section limited by 8-MRs, the pyridine was not able to easily diffuse out as the dome morphology causes the ends of the 10-MRs to be blocked, similar to what has been observed in large zeolite MFI crystals.[10]

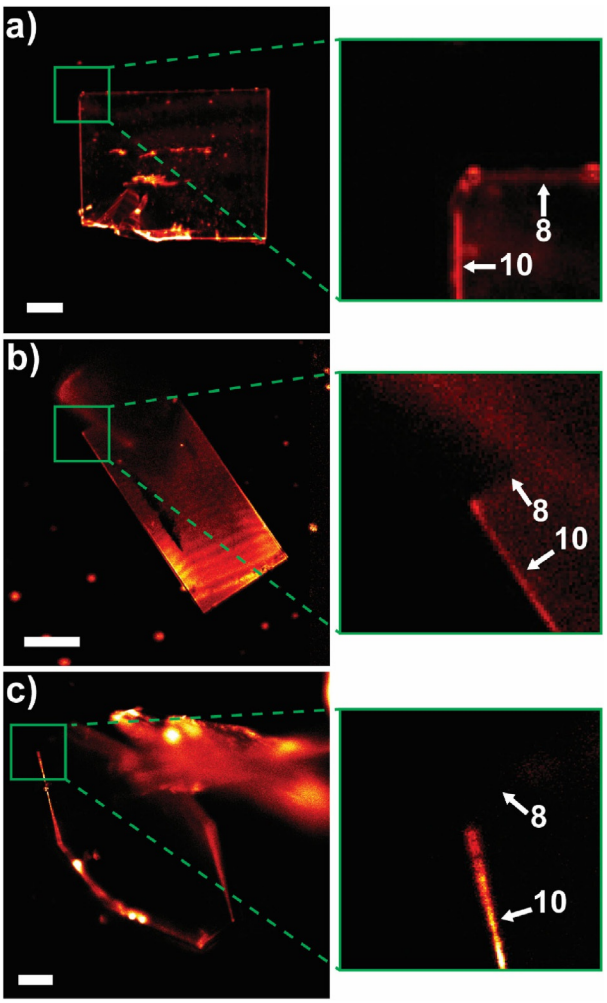

Figure 2. Confocal fluorescence microscopy (CFM) images of calcined zeolite (FER) crystals stained with the fluorescent probe molecule DAMPI. No fluorescence at the intensity of that caused by the DAMPI probe was found in the crystals prior to staining. The direction of the 8- and 10-MRs is indicated in the zoomed-in images on the right. In these images it is clear that more probe molecules are at the 10-MR edge due to the higher fluorescence intensity. a) Purely siliceous FER (**1**) contains obvious mechanical defects that are highlighted by the probe molecule. b) Aluminosilicate FER (**2**), which does not contain any obvious mechanical defects, leading to a uniform background fluorescence across the crystal and highlighting the defect free nature of the growth process. c) Borosilicate FER (**3**), which does not contain any obvious mechanical defects, leading to a uniform background fluorescence across the crystal and highlighting the defect free nature of the growth process. All scale bars represent 50 μm.

The crystal faces of the purely siliceous FER crystals were studied in more detail using AFM, and the results are shown in Figure 3, with a discussion of the method in the Supporting Information Section S5 and additional AFM results in Figures S5 to S8. We were able to determine that the surface of purely siliceous FER is terraced, with an average terrace step height determined to be 9.2 ± 0.6 Å, and an AFM view of the terraced crystal surface along with a graph of the vertical displacement across the surface is shown in Figure 3. As the terraces are steps along the c-axis of the crystal, which has an experimentally determined unit cell length of 18.7 Å (Table S1), they correspond to steps of a half unit cell, which will contain a single layer of intersecting 8- and 10-MRs (Figure 3 d). Finding a half unit cell step height makes it likely that these large zeolite FER crystals grow in a layer-by-layer process where pyridine first fits into partial cavities, which then crystallize around it, forming a completed pore. This is equivalent to the step height measured by AFM, and a schematic of this layer-by-layer growth mechanism is shown in Figure 3 d. Growth in this dimension is much slower than growth in the directions of the 8- and 10-MRs, which is reflected in the plate-like morphology of the crystals. These regular terraces are consistent with a classical crystal growth mechanism where crystals grow via the addition of monomers in solution, which is an interesting finding as zeolites are known to grow by both classical and non-classical mechanisms.[40–43] However, the classical growth mechanism may only apply towards the end of zeolite crystallization as we did not probe the initial stages of crystallization when a non-classical mechanism may apply. Nevertheless, finding a classical growth mechanism, at least at the end of crystallization, is an important observation as these crystals form under seldom investigated solvothermal conditions. There is a prior AFM study of a siliceous FER sample that reported the surface of the material was covered in 'nanowires' that grew parallel to the crystal edges, as if they were on a pyramid, and noted a drop of 10 Å between wires.[44] This terrace height is similar to what we observe in the present study, though we did not find any indication of "nanowire" morphology and observed smooth, flat terrace surfaces (see Figure 3 c).

Large crystals of zeolite FER are able to serve as important model systems to study catalysis and diffusion as their size leads to spatially resolved insights using, e.g., microscopy or intentionally oriented crystals. We demonstrate a facile method to determine pore orientation with respect to crystal habit, as this is known to vary between samples, providing researchers with a powerful, yet simple tool to conduct studies where discrimination between 8- and 10-MRs is critical. The orientation of the 8- and 10-MRs does not correlate with the length or width of the zeolite crystals, meaning the growth rate in these directions is very similar and can vary from synthesis to synthesis. The ability to screen crystals for defects without using damaging and tedious X-ray or electron scattering techniques has been shown with pyrolyzed template molecules as well as fluorescent probe molecules using CFM. The occluded template molecules were determined to reside in the roof section of the crystal, and form triangular shaped patches, indicating the direction of the 8- and 10-MRs. Additionally, the presence of residual coke molecules even after standard calcination procedures offers a warning to ensure complete template removal in any zeolite study. The roof of the crystals was further investigated using AFM, demonstrating a terraced surface, consistent with a layer-by-layer growth mechanism. When combined, these imaging techniques provide a powerful yet facile platform for researchers to continue investigations of large zeolite crystals as they will certainly continue to yield insights into zeolite diffusion and catalysis as well as into their internal architecture.

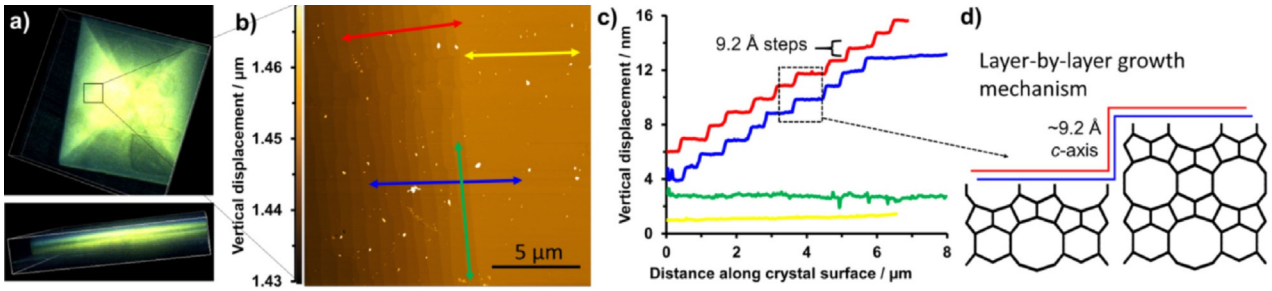

Figure 3. a) Confocal fluorescence microscopy (CFM) images of template containing large purely siliceous FER crystals (**1**) heated in a N_2 atmosphere to 600 °C (ramp 25 °C min^{-1}) in the in situ cell. The bottom image reveals that the fluorescent species exist only in the roof sections of the crystal as significantly lower fluorescence is present in the main body of the material. As the 8-MR openings are along the long edge of the crystal it shows that template molecules are unable to escape the roof portion of the crystal and instead form fluorescent species upon heating. Bounding box dimensions are 255×255×45 µm. Also visible in the top image is birefringence (concentric circles) caused by internal pressure due to occluded organic species that are unable to escape. b) Atomic force microscopy (AFM) image of the surface of purely siliceous FER (**1**) showing four height traces along the surface. c) Vertical displacement along the four height traces on the surface of FER showing regular terrace heights and flat regions. d) Schematic of the FER crystal structure with a step height of ≈9.2 Å along the *c*-axis indicated.

Experimental Section

Details on the large crystals of zeolite FER are given in Table 1. Details of the single crystal X-ray diffraction (XRD), atomic force microscopy (AFM), probe molecules, confocal fluorescence microscopy (CFM), high-temperature in situ microscopy, wide-field optical microscopy and scanning electron microscopy (SEM) are all provided in the Supporting Information. Additionally, a cif file for the full refinement of **1** is included in the Supporting Information.

Abbreviations

AFM	atomic force microscopy
CFM	confocal fluorescence microscopy
DAMPI	*trans*-4-(4′-(N,N-dimethylamino)styryl)-N-methylpyridinium iodide
MRs	membered rings
SEM	scanning electron microscopy
TGA	thermogravimetric analysis

Acknowledgements

We would like to thank the Professor Mark E. Davis lab (Caltech, Pasadena, USA) for providing the sample of purely siliceous FER and Professor Jens Weitkamp (University of Stuttgart, Stuttgart, Germany) and Professor Jörg Kärger (University of Leipzig, Leipzig, Germany) for providing the aluminosilicate and borosilicate samples. We would like to thank Dr. Ingmar Swart (Utrecht University) for the use of the AFM. This work is supported by the NWO Gravitation program, Netherlands Center for Multiscale Catalytic Energy Conversion (MCEC), and a European Research Council (ERC) Advanced Grant (no. 321140). J.S. has received funding from the European Union's Horizon 2020 research and innovation programme under the Marie Sklodowska-Curie grant agreement No 702149.

Keywords: atomic force microscopy · confocal fluorescence microscopy · ferrierite · intergrowth structure · zeolites

[1] A. M. Beale, F. Gao, I. Lezcano-Gonzalez, C. H. F. Peden, J. Szanyi, *Chem. Soc. Rev.* **2015**, *44*, 7371 – 7405.
[2] J. Shi, Y. Wang, W. Yang, Y. Tang, Z. Xie, *Chem. Soc. Rev.* **2015**, *44*, 8877 – 8903.
[3] J. Coronas, *Chem. Eng. J.* **2010**, *156*, 236 – 242.
[4] M. E. Davis, *Chem. Mater.* **2014**, *26*, 239 – 245.
[5] M. E. Davis, R. F. Lobo, *Chem. Mater.* **1992**, *4*, 756 – 768.
[6] M. E. Davis, *Nature* **2002**, *417*, 813 – 821.
[7] W. Vermeiren, J.-P. Gilson, *Top. Catal.* **2009**, *52*, 1131 – 1161.
[8] O. Ugurlu, J. Haus, A. A. Gunawan, M. G. Thomas, S. Maheshwari, M. Tsapatsis, K. A. Mkhoyan, *Phys. Rev. B: Condens. Matter Mater. Phys.* **2011**, *83*, 113408.
[9] B. M. Weckhuysen, *Angew. Chem. Int. Ed.* **2009**, *48*, 4910 – 4943; *Angew. Chem.* **2009**, *121*, 5008 – 5043.
[10] L. Karwacki, M. H. F. Kox, D. A. Matthijs de Winter, M. R. Drury, J. D. Meeldijk, E. Stavitski, W. Schmidt, M. Mertens, P. Cubillas, N. John, A. Chan, N. Kahn, S. R. Bare, M. Anderson, J. Kornatowski, B. M. Weckhuysen, *Nat. Mater.* **2009**, *8*, 959 – 965.
[11] I. L. C. Buurmans, B. M. Weckhuysen, *Nat. Chem.* **2012**, *4*, 873 – 886.
[12] D. Mores, E. Stavitski, M. H. F. Kox, J. Kornatowski, U. Olsbye, B. M. Weckhuysen, *Chem. Eur. J.* **2008**, *14*, 11320 – 11327.
[13] D. Mores, J. Kornatowski, U. Olsbye, B. M. Weckhuysen, *Chem. Eur. J.* **2011**, *17*, 2874 – 2884.
[14] E. Stavitski, M. H. F. Kox, B. M. Weckhuysen, *Chem. Eur. J.* **2007**, *13*, 7057 – 7065.
[15] L. R. Aramburo, L. Karwacki, P. Cubillas, S. Asahina, D. A. M. de Winter, M. R. Drury, I. L. C. Buurmans, E. Stavitski, D. Mores, M. Daturi, P. Bazin, P. Dumas, F. Thibault-Starzyk, J. A. Post, M. W. Anderson, O. Terasaki, B. M. Weckhuysen, *Chem. Eur. J.* **2011**, *17*, 13773 – 13781.
[16] A. Kuperman, S. Nadimi, S. Oliver, G. A. Ozin, J. M. Garcés, M. M. Olken, *Nature* **1993**, *365*, 239 – 242.
[17] J. E. Lewis, G. R. Gavalas, M. E. Davis, *AIChE J.* **1997**, *43*, 83 – 90.
[18] P. Kortunov, L. Heinke, S. Vasenkov, C. Chmelik, D. B. Shah, J. Kärger, R. A. Rakoczy, Y. Traa, J. Weitkamp, *J. Phys. Chem. B* **2006**, *110*, 23821 – 23828.
[19] J. Kärger, P. Kortunov, S. Vasenkov, L. Heinke, D. B. Shah, R. A. Rakoczy, Y. Traa, J. Weitkamp, *Angew. Chem. Int. Ed.* **2006**, *45*, 7846 – 7849; *Angew. Chem.* **2006**, *118*, 8010 – 8013.
[20] L. Heinke, C. Chmelik, P. Kortunov, D. M. Ruthven, D. B. Shah, S. Vasenkov, J. Kärger, *Chem. Eng. Technol.* **2007**, *30*, 995 – 1002.
[21] F. Hibbe, V. R. R. Marthala, C. Chmelik, J. Weitkamp, J. Kärger, *J. Chem. Phys.* **2011**, *135*, 184201.
[22] J. Kärger, T. Binder, C. Chmelik, F. Hibbe, H. Krautscheid, R. Krishna, J. Weitkamp, *Nat. Mater.* **2014**, *13*, 333 – 343.
[23] S. C. C. Wiedemann, Z. Ristanović, G. T. Whiting, V. R. Reddy Marthala, J. Kärger, J. Weitkamp, B. Wels, P. C. A. Bruijnincx, B. M. Weckhuysen, *Chem. Eur. J.* **2016**, *22*, 199 – 210.
[24] V. R. R. Marthala, M. Hunger, F. Kettner, H. Krautscheid, C. Chmelik, J. Kärger, J. Weitkamp, *Chem. Mater.* **2011**, *23*, 2521 – 2528.
[25] R. A. Rakoczy, Y. Traa, P. Kortunov, S. Vasenkov, J. Kärger, J. Weitkamp, *Microporous Mesoporous Mater.* **2007**, *104*, 179 – 184.

[26] Z. Li, M. C. Johnson, M. Sun, E. T. Ryan, D. J. Earl, W. Maichen, J. I. Martin, S. Li, C. M. Lew, J. Wang, M. W. Deem, M. E. Davis, Y. Yan, *Angew. Chem. Int. Ed.* **2006**, *45*, 6329 – 6332; *Angew. Chem.* **2006**, *118*, 6477 – 6480.
[27] J. E. Lewis, C. C. Freyhardt, M. E. Davis, *J. Phys. Chem.* **1996**, *100*, 5039 – 5049.
[28] Z. A. D. Lethbridge, D. S. Keeble, D. Walker, P. A. Thomas, R. I. Walton, *J. Appl. Crystallogr.* **2010**, *43*, 168 – 175.
[29] A. B. Pinar, P. A. Wright, L. Gómez-Hortigüela, J. Pérez-Pariente, *Microporous Mesoporous Mater.* **2010**, *129*, 164 – 172.
[30] R. E. Morris, S. J. Weigel, N. J. Henson, L. M. Bull, M. T. Janicke, B. F. Chmelka, A. K. Cheetham, *J. Am. Chem. Soc.* **1994**, *116*, 11849 – 11855.
[31] S. J. Weigel, J.-C. Gabriel, E. G. Puebla, A. M. Bravo, N. J. Henson, L. M. Bull, A. K. Cheetham, *J. Am. Chem. Soc.* **1996**, *118*, 2427 – 2435.
[32] I. Bull, P. Lightfoot, L. A. Villaescusa, L. M. Bull, R. K. B. Gover, J. S. O. Evans, R. E. Morris, *J. Am. Chem. Soc.* **2003**, *125*, 4342 – 4349.
[33] R. J. Darton, P. Wormald, R. E. Morris, *J. Mater. Chem.* **2004**, *14*, 2036 – 2040.
[34] R. J. Darton, R. E. Morris, *Solid State Sci.* **2006**, *8*, 342 – 345.
[35] L. Karwacki, E. Stavitski, M. H. F. Kox, J. Kornatowski, B. M. Weckhuysen, *Angew. Chem. Int. Ed.* **2007**, *46*, 7228 – 7231; *Angew. Chem.* **2007**, *119*, 7366 – 7369.
[36] L. Karwacki, B. M. Weckhuysen, *Phys. Chem. Chem. Phys.* **2011**, *13*, 3681 – 3685.
[37] L. Karwacki, H. E. Van Der Bij, J. Kornatowski, P. Cubillas, M. R. Drury, D. A. De Matthijs Winter, M. W. Anderson, B. M. Weckhuysen, *Angew. Chem. Int. Ed.* **2010**, *49*, 6790 – 6794; *Angew. Chem.* **2010**, *122*, 6942 – 6946.
[38] F. C. Hendriks, D. Valencia, P. C. A. Bruijnincx, B. M. Weckhuysen, *Phys. Chem. Chem. Phys.* **2017**, *19*, 1857 – 1867.
[39] F. C. Hendriks, J. E. Schmidt, J. A. Rombouts, K. Lammertsma, P. C. A. Bruijnincx, B. M. Weckhuysen, *Chem. Eur. J.* **2017**, *23*, 6305 – 6314.
[40] K. N. Olafson, R. Li, B. G. Alamani, J. D. Rimer, *Chem. Mater.* **2016**, *28*, 8453 – 8465.
[41] A. I. Lupulescu, J. D. Rimer, *Science* **2014**, *344*, 729 – 732.
[42] M. Kumar, H. Luo, Y. Román-Leshkov, J. D. Rimer, *J. Am. Chem. Soc.* **2015**, *137*, 13007 – 13017.
[43] M. Kumar, R. Li, J. D. Rimer, *Chem. Mater.* **2016**, *28*, 1714 – 1727.
[44] M. W. Anderson, J. R. Agger, N. Pervaiz, S. J. Weigel, A. K. Cheetham in *12th Int. Zeolite Conf.* (Ed.: Treacy), **1999**, pp. 1487 – 1494.

Manuscript received: May 25, 2017
Revised manuscript received: July 1, 2017
Version of record online: August 15, 2017

